COASTAL CAROLINA
UNIVERSITY

Office of Sponsored Programs
and Research Services

843.349.2978
843.234.0441 fax
OSPRS@coastal.edu

March 31, 2017

Defense Technical Information Center
8725 John J. Kingman Road
Suite 0944
Fort Belvoir, VA 22060-6218

To Whom It May Concern,

Enclosed please find the Final Technical Report with SF 298 for Dr. Erin E. Hackett's ONR grant entitled *Radar Measurements of Ocean Surface Waves Using Proper Orthogonal Decomposition*.

If you have any questions regarding the submission of this report, please reach out to me at your convenience at (843) 349-5030 or via email at scassavau@coastal.edu. Should you have specific programmatic questions, Dr. Hackett is also available to discuss at your request.

Sincerely,

Stephanie Cassavaugh, Director

Enclosures

P.O. Box 261954
Conway, South Carolina
29528-6054

Radar Measurements of Ocean Surface Waves Using Proper Orthogonal Decomposition

Erin E. Hackett, Ph.D.
Coastal Carolina University
Department of Coastal and Marine Systems Science
P.O. Box 261954 Conway, SC, 29528
443.677.6964 Cell
843.349.4087 Phone
843.349.4042 Fax
ehackett@coastal.edu

Final Report – Award: N00014-15-1-2044 (331 [Hess III, Paul])

REPORT DOCUMENTATION PAGE

Form Approved
OMB No. 0704-0188

The public reporting burden for this collection of information is estimated to average 1 hour per response, including the time for reviewing instructions, searching existing data sources, gathering and maintaining the data needed, and completing and reviewing the collection of information. Send comments regarding this burden estimate or any other aspect of this collection of information, including suggestions for reducing the burden, to Department of Defense, Washington Headquarters Services, Directorate for Information Operations and Reports (0704-0188), 1215 Jefferson Davis Highway, Suite 1204, Arlington, VA 22202-4302. Respondents should be aware that notwithstanding any other provision of law, no person shall be subject to any penalty for failing to comply with a collection of information if it does not display a currently valid OMB control number.
PLEASE DO NOT RETURN YOUR FORM TO THE ABOVE ADDRESS.

1. REPORT DATE *(DD-MM-YYYY)*	2. REPORT TYPE	3. DATES COVERED *(From - To)*
30-03-2017	Final Technical	22-01-2015 - 31-12-2016

4. TITLE AND SUBTITLE
Radar Measurements of Ocean Surface Waves using Proper Orthogonal Decomposition

5a. CONTRACT NUMBER

5b. GRANT NUMBER
N00014-15-1-2044

5c. PROGRAM ELEMENT NUMBER

6. AUTHOR(S)
Hackett, Erin, E., Ph.D.

5d. PROJECT NUMBER

5e. TASK NUMBER

5f. WORK UNIT NUMBER

7. PERFORMING ORGANIZATION NAME(S) AND ADDRESS(ES)
Coastal Carolina University
PO Box 261954
Conway, SC 29528-6054

8. PERFORMING ORGANIZATION REPORT NUMBER

9. SPONSORING/MONITORING AGENCY NAME(S) AND ADDRESS(ES)
Office of Naval Research
Ship Systems and Engineering Research Division (ONR 331)
875 N. Randolph Street
Arlington, VA 22203-1995

10. SPONSOR/MONITOR'S ACRONYM(S)
ONR

11. SPONSOR/MONITOR'S REPORT NUMBER(S)

12. DISTRIBUTION/AVAILABILITY STATEMENT
Approved for Public Release; Distribution is Unlimited.

13. SUPPLEMENTARY NOTES

14. ABSTRACT
Current methods to extract information about the ocean surface wave field from radar measurements primarily rely on use of Fourier transforms (FFT) and filtering spectra on the linear dispersion relationship for ocean surface waves. This report discusses development and evaluation of the use of proper orthogonal decomposition (POD) as an alternative method. Results show similar performance of conventional FFT-based techniques and POD methods for estimation of wave statistics; however, evaluations show improved performance of the POD method for phase-resolved wave fields, particularly for wave fields with high energy off the linear dispersion relationship.

15. SUBJECT TERMS
Sea clutter, remote sensing, ocean surface waves, Fourier transforms, Proper orthogonal decomposition

16. SECURITY CLASSIFICATION OF:			17. LIMITATION OF ABSTRACT	18. NUMBER OF PAGES	19a. NAME OF RESPONSIBLE PERSON
a. REPORT	b. ABSTRACT	c. THIS PAGE			Erin E. Hackett
					19b. TELEPHONE NUMBER *(Include area code)*
U	U	U	UU	21	843-349-4087

Radar Measurements Of Ocean Surface Waves Using Proper Orthogonal Decomposition

Erin Hackett
Department of Coastal and Marine Systems Science
P.O. Box 261954 Conway, SC, 29528
phone: 843-349-4087
fax: 843-349-4042
email: ehackett@coastal.edu

Award Number: N00014-15-1-2044

LONG-TERM GOALS

Current state-of-the-art techniques for measurement of ocean surface waves based on radar measurements predominantly use Fourier transforms (FFTs) to extract information about the ocean surface wave field from the measured signal (e.g., Young et al., 1985). In addition, the methods often rely on filtering the FFT of radar backscatter or Doppler velocities using the linear dispersion relationship for surface gravity waves to remove artifacts associated with the measurement (e.g., "sea spikes"). Because natural wave fields are neither linear nor stationary, one might raise the question of whether FFTs are the optimal tool? Furthermore, when the end-goal of the wave retrieval is space- and time-resolved sea surface elevation maps (i.e., rather than a wave spectrum), the back-and-forth translations between Fourier and spatiotemporal domains can introduce artifacts and impose additional sensing requirements that would not exist if data were processed exclusively in the spatiotemporal domain. The long-term goal of this research is to improve and explore alternative signal processing methods to extract ocean wave fields from sea clutter. Advancement of these techniques enables accurate sea surface elevation maps surrounding ships, offshore platforms, and shorelines to be produced. These maps can provide important information regarding sea conditions to inform operational decisions such as intra- and inter-ship transfers, small-boat launch and recovery, and helicopter landings. Such detailed sea state information generally improves the fleet's maritime domain awareness.

OBJECTIVES

The objective of this research is to develop and evaluate the use of proper orthogonal decomposition (POD) for wave field retrieval from radar Doppler measurements. Specifically, the following sub-objectives enable this objective to be achieved:

(i) Determine whether the basis functions of the POD of Doppler measurements have physical significance that can be associated with the wave field
(ii) Develop methodology for applying POD to data obtained with a rotating radar system
(iii) Compare the wave field retrievals obtained via POD to those obtained with conventional FFT and dispersion curve filtering techniques
(iv) Compare both results of (iii) to ground truth sensors (i.e., wave buoys), both in-terms of wave statistics as well as phase-resolved comparisons, when possible.

APPROACH

Radar returns from the sea surface are complex and contain contributions from the environment (e.g., wind, waves, currents) as well as artifacts associated with electromagnetic (EM) (wave) propagation (e.g., multipath, multibounce, shadowing, "sea spikes"). Most methods for processing sea clutter data for extraction of wave field information utilize three-dimensional (3D) fast Fourier transforms (FFTs) (Young et al., 1985). Typically, these 3D spectra are subsequently filtered based on the linear dispersion relationship for surface gravity waves to remove contributions deemed to be not associated with the wave field. Oceanic wave fields, particularly in high sea states, are not linear or stationary, and therefore, application of linear, stationary techniques such as FFTs may not be best suited for this application. They are often used because of simplicity of their application and a lack of alternative options. Furthermore, at least a portion of the nonlinear wave field does not lie on the dispersion curve, and thus, filtering the Doppler spectrum based on the linear dispersion curve undoubtedly discards part of the wave field information. Nonlinear ocean wave and EM propagation effects overlap too much in frequency-wavenumber space to separate them using these current techniques. For example, Figure 1 shows a typical wavenumber-frequency spectrum computed from (radar) Doppler measurements. The dashed white line in the figure is the linear dispersion curve for surface gravity waves: $\omega = \vec{u}_c \cdot \vec{k} + \sqrt{gktanh(kh)}$, where $\vec{u}_c$ is the surface current, g is acceleration due to gravity, $\vec{k}$ is wavenumber (and k is wavenumber magnitude), and h is water depth. In Figure 1, the primary energy peaks lie on the dispersion curve; one peak for swell and another for wind seas. In addition to this energy, the presence of the first harmonic is evident above the main energy peaks (on the dispersion curve), and clearly there is a broad spectral distribution of energy at frequencies and wavenumbers smaller than that associated with the dispersion curve (hereafter referred to as the "group line"). The latter contains contributions from the nonlinear portion of the wave field (e.g., wave breaking), EM effects (e.g., shadowing), and interference between wave systems (Plant and Farquharson, 2012; Nieto Borge et al., 2004; Smith et al., 1996). All these contributions to the signal are removed with the procedure of filtering the spectrum based on the dispersion curve denoted with the dotted lines in Figure 1. This procedure may be sufficient for obtaining general information about the wave field directionality and frequency content, but the accuracy of time-space resolved sea surface elevation maps is unclear when constructed from inverse FFTs after some wave field contributions have been neglected. For Navy applications, this shortcoming could be significant because it is measurement/prediction of the anomalous/large wave event that is the most critical.

This research evaluates use of proper orthogonal decomposition (POD) to separate and extract the wave field information from the measured signal. This technique can be applied to non-stationary and nonlinear processes, and is also referred to as principal component analysis (PCA), Karhunen-Loéve decomposition/transform, or singular value decomposition (SVD). In general, it is used to obtain a low-dimensional approximation for high-dimensional processes, such as chaotic systems (Chatterjee, 2000). Although the method is a linear technique, it is optimal relative to other linear techniques, such as FFTs, for representation of nonlinear processes and has been applied extensively in the areas of turbulence and image processing (Kerschen and Golinval, 2002). Although there is no physical basis/interpretation inherent to the method because it is purely a mathematical tool, there has been an increasing body of work in several different research areas suggesting that POD can be linked with physical interpretations (e.g., Diamessis et al., 2010; Kerschen and Golinval, 2002; Hackett et al., 2014).

The central idea in POD is that a signal, $S(r,t)$, can be represented by a set of modes, $\varphi_k(r)$, and coefficient functions, $c_k(t)$:

$$S(r,t) = \sum_{k=1}^{M} c_k(t)\phi_k(r) \qquad (1)$$

such that as M→∞ the true signal is reconstructed exactly by the summation. It is the choice of the basis functions or modes that differentiates POD from other methods. Instead of choosing the basis functions *a priori*, e.g., sines and cosines, Legendre polynomials, etc., they are determined from the data itself. They are orthonormal and minimize the number of modes required to account for the majority of the variance in the signal. For example, they are chosen such that a three mode (k=3) approximation is the best possible 3-mode approximation, and the same for four modes, five, and so-on. This particular selection of modes is referred to as the proper orthogonal modes, which can be computed from a singular value decomposition of the signal. The idea is that inclusion or neglect of certain modes can act as a filter on the signal enabling different aspects of the wave field to be retrieved. This mode selection could permit an improved wave field extraction by including content associated with the wave field that does not lie on the dispersion curve. In Eqn (1), the signal, S, is a function of range and time, but the same method can be applied for any 2D configuration, for example two spatial coordinates.

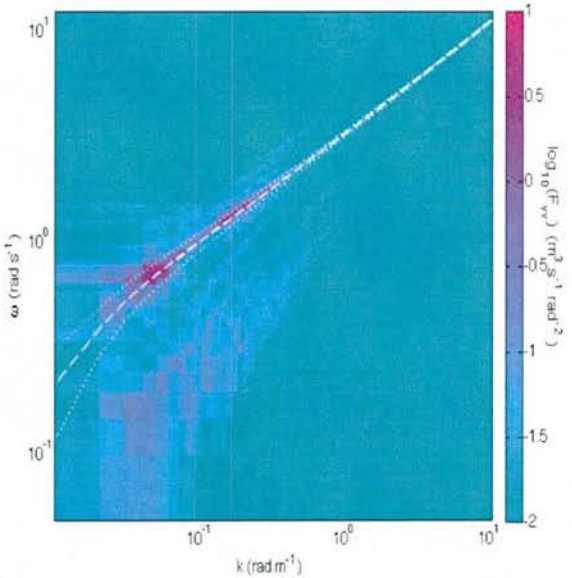

Figure 1: Power spectral density of Doppler velocities (F_{vv}). The white dashed line is the linear dispersion curve for ocean surface waves and the white dotted lines show the width of a typical dispersion curve filter.

There are also a number of other potential advantages to this technique over FFT processing. First, translation between Fourier and spatiotemporal domains requires application of windowing functions, which can introduce artifacts into the data, and these translations also impose certain sensing requirements because the sample interval and length of the time/spatial series sets the frequency/wavenumber resolution, minimum frequency, and Nyquist limit. Using the POD technique, all the data remains in the spatiotemporal domain for all the computations; thus, introduction of

artifacts is minimized and sensing requirements could be relaxed. Second, sea surface elevation maps and/or raw radar measurements can be saved much more efficiently in-terms of data storage, and the POD method is computationally less intensive than FFTs. It is also feasible that by neglecting certain modes in the reconstructed signal that are due to noise, a cleaner signal can be used for the FFT analysis thereby improving results obtained by FFT methods.

Prior research has shown viability of POD based-on results of application of POD to modeled wave fields of various complexity (Hackett et al., 2014). This prior research has not included any radar artifacts (e.g., shadowing, range-dependent noise, multipath, etc.) into the simulated wave data; thus, these results assume a "perfect" radar performance. Thus, the proposed research would extend this research to examine the impact of such artifacts. Furthermore, the technique has not yet been applied to rotating or staring radar-based wave measurements, which is a primary focus of this effort.

The results from the method are compared to those from conventional FFT-based processing that filters on the dispersion relationship for surface gravity waves. Both the FFT-based and POD-based results are also compared to ground truth sensors (i.e., wave buoys), both in terms of wave statistics and phase-resolved comparisons, when possible. The data used for these comparisons come from two different tests completed by performers under the *Environmental and Ship Motion Forecasting* (ESMF) ONR FNC program (Alford et al., 2015; Connell et al., 2015), an experiment performed by the *Naval Surface Warfare Center Carderock Division* (NSWCCD) at the *Scripps Institution of Oceanography* pier (SIO) (Hackett et al., 2015) for the ESMF program, and radar emulator results generated by Gordon Farquharson at the *University of Washington Applied Physics Laboratory* (also partly developed under the ESMF program). Thus, the results span a variety of environmental conditions and radar systems. An overview of the three radar systems evaluated as well as the environmental conditions during the various experiments are provided in Tables 1, 2, and 3 (for the datasets used in this study). The emulated radar data was produced using a wave directional spectrum that is similar to the conditions of dataset 13 in Table 3 and a modeled antenna that is the same as the UM radar system (see Table 1). Multiple emulator runs were produced using the same wave directional distributions with H_s and V_{rms} similar to the values in Table 3 for dataset 13 as well as with H_s and V_{rms} slightly smaller than that shown in the table.

Table 1: Radar parameters for Doppler measurements for the three radars examined in this study: center frequency (f_c), bandwidth (Δf), polarization, range resolution, range footprint (range covered), pulse repetition frequency (PRF), and rotation rate. Note that the information for the APS radar is for one of four antennas that each covers one quarter of an entire radar frame (i.e., 360 deg in azimuth).

Radar System	f_c (GHz)	Δf (MHz)	Polarization	Resolution (m)	Radar Footprint (m)	PRF (Hz)	Rotation Rate (RPM)
DREAM	9.30	500	VV	0.30	615	800	0
UM	9.41	30	VV	3.75	960	2000	24
APS*	9.20	28	VV	4.80	998	25000	5
*one of the four APS antennas							

Table 2: Wave field and other environmental conditions for two SIO pier experimental datasets examined in this study. H_s is significant wave height, T is mean wave period, T_p is peak wave period, θ_p is peak wave direction, θ_w is wind direction, and U_W is wind speed (Hackett et al., 2015).

Run	Date	Radar Time	H_s (m)	T (s)	Θ_p (°)	T_p (s)	Θ_w (°)	U_w (m/s)
246	7/27/2010	21:34	0.60	7.0	282	9.8	297	3.9
269	7/29/2010	20:22	0.62	5.1	296	5.2	296	3.9

WORK COMPLETED

The work completed under this grant involves several main components: (i) evaluation of any physical connection of POD basis functions to the wave field, (ii) development of a procedure for applying the POD method to rotating radar system data, (iii) comparison of results of POD method with conventional FFT-based methods over a variety of environmental conditions and for multiple radar systems, and (iv) comparison of both methods to ground truth sensors. More details regarding each of these components are provided in the following subsections as well as in Kammerer (2017).

Table 3: Rotating radar datasets examined in this study. Information includes: dataset number, test associated with the data collected, date and time of data collection, availability of APS radar system and UM radar system data, buoy measured environmental conditions (H_s: significant wave height, λ_p: peak wavelength, V_{rms}: RMS of orbital velocity, and number of wave systems), directional spread between swell and wind waves ($\Delta\theta$) as applicable and measured by the radars, and ship (anemometer) measured wind speed, U_w.

Dataset	Test	Date	Time	APS	UM	H_s (m)	U_w (m/s)	λ_p (m)	V_{rms} (m/s)	Wave Systems	$\Delta\Theta$ (°)
1*	CK15	17-May-15	20:08:00	✓	✓	0.10	6.0	167	0.03	2	53
2++	CK15	17-May-15	21:20:00	×	✓	0.19	7.5	111	0.09	1	0
3	Melville	15-Sep-13	17:10:40	✓	✓	1.62	12	105	0.39	1	0
4++	Melville	16-Sep-13	1:36:00	✓	✓	1.42	15	95	0.46	1	0
5*	Melville	16-Sep-13	15:43:00	✓	✓	1.29	11	82	0.43	2	23
6*	Melville	16-Sep-13	18:29:32	✓	✓	1.29	12	98	0.44	2	50
7	Melville	17-Sep-13	0:08:45	✓	✓	1.65	11	77	0.54	2	41
8	Melville	17-Sep-13	0:33:34	✓	✓	1.48	11	78	0.49	2	46
9	Melville	17-Sep-13	0:58:10	✓	✓	1.68	11	78	0.52	2	44
10	Melville	17-Sep-13	2:00:00	✓	✓	1.59	12	92	0.51	2	30
11**	CK15	17-May-15	22:20:00	×	✓	1.64	7.0	111	0.53	2	61
12+	CK15	21-May-15	20:32:00	✓	✓	1.07	2.3	97	0.28	1	0
13+	Melville	17-Sep-13	14:28:53	✓	✓	2.10	8.9	108	0.63	2	59
14**	Melville	17-Sep-13	19:27:33	✓	✓	2.15	9.9	105	0.63	2	0

* Lowest H_s for respective test
\+ Lowest U_w for respective test
** Highest H_s for respective test
++ Highest U_w for respective test

Physical Significance of POD Modes

POD mode basis functions are derived from the data *a posteriori*; thus, they are not restricted to sines and cosines as in Fourier methods. The interpretation of POD mode functions however, is more complex than Fourier methods, as there is no inherent physical interpretation of the mode functions. This subsection examines the physical interpretation of the POD basis functions as applied to Doppler radar measurements of the ocean surface. Mode basis functions from applying POD to data acquired from an emulated rotating radar, rotating radar, and staring (or non-rotating) radar are examined.

First, the physical interpretation of POD mode functions as related to wave-field physics from the staring radar SIO experiment are examined. This experiment was chosen to examine first because the data format (i.e., $\boldsymbol{D}(r,t)$) most closely matches the simulated idealized radar data from 2D wave-fields examined in Hackett et al. (2014), which showed that leading POD modes of this simulated data shared characteristics of the wave-field physics. To investigate the effect of the number of wave systems present, two datasets were selected to examine. Dataset 246 was collected under mixed seas with both swell and wind-wave energy present, while dataset 269 was collected during wind sea only conditions (also see Table 2).

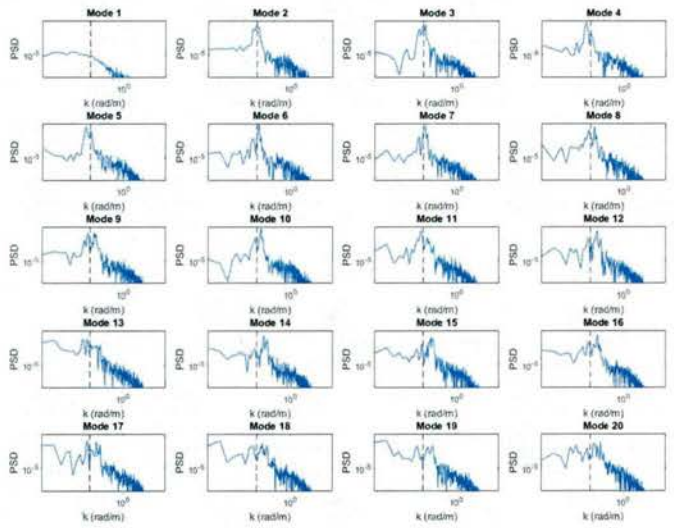

Figure 2: Power spectral densities (PSD) of the leading 20 modes computed from POD applied to spatiotemporal Doppler velocity distributions (dataset 269 from NSWCCD's SIO pier experiment).

Figure 2 shows the 1D power spectral densities (PSD) (or energy spectrum) of each of the leading twenty mode functions from POD applied to spatiotemporal Doppler velocity for dataset 269 during wind sea only conditions. The vertical dashed line shows the peak wavenumber during the time period that the data was collected. All of the leading modes, with the exception of mode one, show spectral peaks at or surrounding the peak wavelength, which indicates that a significant portion of the variance of the mode function is associated with wavelengths near the waves' peak wavelength. Figure 3 shows the second mode function, further confirming that the function is oscillatory with a wavelength that is similar to the peak wavelength of the measured wave-field. These results suggest that under uni-modal sea conditions the leading POD mode functions are oscillatory and oscillate at similar wavelengths as the peak wavelength of the measured wave-field and thus have clear correspondence to the physics of the measured wave-field. Also note from Figure 2 that aside from the first mode (that is interpreted to be associated with a large scale trend, such as the range-dependent signal decay), the magnitude of the spectral peak near the peak wavelength is greatest in the smallest modes and decreases and broadens as the mode number increases. This result implies that the smallest modes are more tightly coupled to the

wave field physics than higher modes. Similar results were found for run 246 during mixed sea conditions. From those results, it can be deduced that mixed seas do not significantly change the ordering of the basis functions and in a mixed sea scenario the basis functions incorporate both swell and wind-seas in the same functions.

In order to evaluate if the POD method preferentially reconstructs wave energy as opposed to non-wave contributions to the radar Doppler measurement, energy in each n mode reconstruction is examined as well as energy only inside swell and wind-wave spectral "bands". Figure 4 shows total reconstructed energy, as well as energy within only the swell and wind-wave energy bands, in each n mode reconstruction. For each n mode reconstruction, modes 1 through n are used for reconstruction. The PSD of velocity is calculated for each POD mode velocity reconstruction and integrated twice to compute energy captured by that reconstruction. The swell and wind-wave wavelength bands are based on the width of the spectral energy peaks of the original Doppler velocity data associated with the swell and wind-waves for each data set. Specifically, the swell energy wavelength band is defined as wavelengths from 87 m to 210 m, and the wind-wave band is defined as wavelengths from 20 m to 70 m. The vertical axis in Figure 4 shows percentage of total energy. The results in this figure show that the POD mode reconstructions accumulate energy from within the swell and wind-wave wavenumber bands at a faster rate than total energy is accumulated. The reconstruction of modes 1-20 represents 70% of the swell and wind-wave energy, but only 28% of the total energy. The reconstruction of modes 1-100 represents 99% of the energy in the swell and wind wave spectral bands. This result demonstrates that a leading mode reconstruction would contain more energy in the wave bands than energy outside of these bands, where the latter could be associated with potential non-wave contributions to the radar measurement.

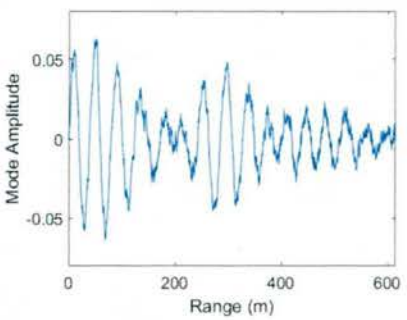

Figure 3: Second mode function from decomposition of spatiotemporal Doppler velocity from dataset 269.

The mode basis functions of emulated rotating radar data were also examined to determine if the mode basis functions correspond to the physics of the measured wave-field. The rotating radar data differs from the staring radar data because the Doppler velocity is a function of two spatial coordinates (i.e., $\boldsymbol{D}(x,y)$) rather than range and time (i.e., $\boldsymbol{D}(r,t)$) and therefore it cannot be assumed *a priori* that the basis functions derived from the POD method will be the same for the rotating and staring radars. However, the Doppler data are first rotated so that the predominant wave propagation is along the x-direction, which is the same direction that the mode functions are associated (see next subsection for further details). Due to this rotation, similar behavior as observed with the starting radar is expected.

Figure 5a shows the first mode basis function of POD applied to a frame of emulated rotating radar Doppler velocity data. This figure shows that the mode function is oscillatory and Figure 5b shows the PSD of this mode where it can be seen that the mode's spectral peaks are consistent with the peak wavelengths from the directional wave spectrum from which the emulator run was initiated.

Figure 6 shows the 1D wavenumber spectrum for each individual mode reconstruction for POD applied to a frame of Doppler velocity data measured using the rotating radar developed by the *University of Michigan* (UM) under the ESMF program. The 2D (k_x-k_y) spectrum is calculated from the individual mode velocity reconstructions and integrated over k_y to yield a 1D wavenumber spectrum

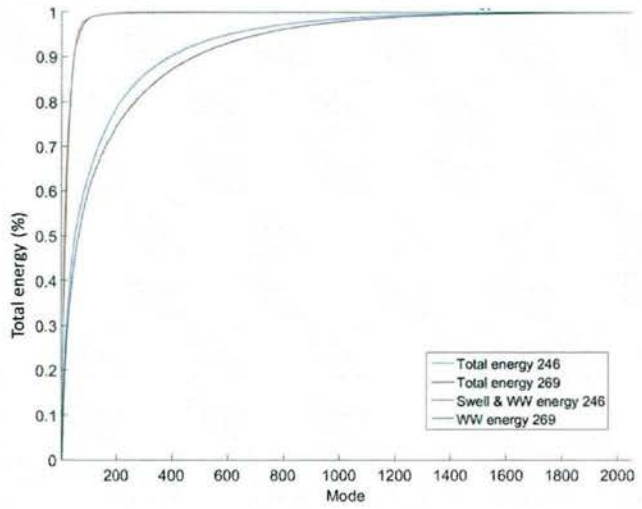

Figure 4: Normalized cumulative energy versus *n* mode reconstruction, and normalized cumulative energy within swell and wind-wave (WW) wavelength bands. Swell and wind-wave energy is accumulated at a faster rate than total energy.

physical significance in relation to the wave field.

for each mode reconstruction. The vertical dashed white line represents the peak wavelength during the time when the dataset was collected. Energy based-on mode 1 through 10 velocity reconstructions is largest around the peak wavelength. Above the mode 10 reconstruction, small amounts of energy are spread across the remaining reconstructions and across many wavelengths. This energy is presumably part of non-wave contributions to the radar Doppler velocity measurement. Note that the UM rotating radar range resolution is much coarser than the staring DREAM radar (see Table 1).

From these results, we conjecture that the POD performs similarly for the rotating radar as the staring radar in that the leading POD mode functions are oscillatory and have wavelengths representative of the measured wave field and therefore, have a clear

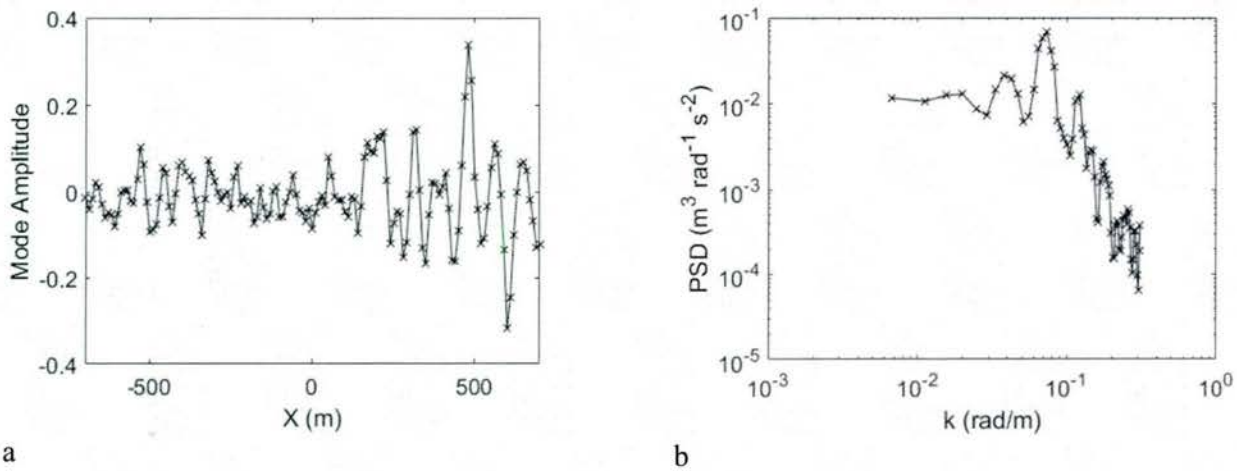

a b

Figure 5: (a) First mode function from POD applied to a single frame of emulated rotating radar Doppler velocity measurements. (b) Wavenumber spectrum of the first POD mode function presented in (a).

Method Development of POD Applied to Rotating Radar Data

Because prior research has applied POD to 2D Doppler distributions in range and time only (Hackett et al., 2014), the method had to be adapted in order to generate time-space resolved wave orbital velocity maps based on Doppler measurements from rotating radar. This section provides an overview of the method developed. First, several data preparation steps are performed:

(i) Translate data from a ship-based coordinate system into a geo-referenced East-North coordinate system
(ii) Detrend the data along each azimuth
(iii) Compute the directional wave spectrum and determine the peak wave direction
(iv) Rotate the original Doppler frame to translate the peak wave direction to the East-West direction
(v) Convert to a Cartesian coordinate system (waves now propagating along the x-direction)
(vi) Insert zeroes in any blanking region dictated by a minimum range of the radar

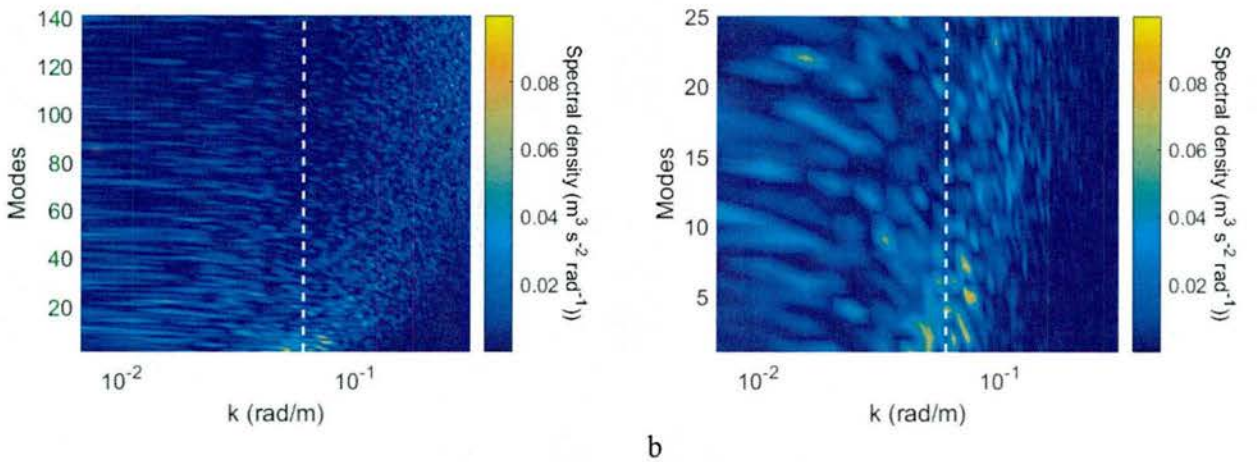

Figure 6: Integrated 2D wavenumber spectra of individual mode velocity reconstructions versus mode number for rotating UM radar. (a) shows the full range of POD modes and (b) shows a zoom-in of the leading 25 modes.

Once these preparatory steps have been completed, then the application of the POD method is performed. The POD method takes a signal, in the case of the rotating radar data, one Doppler velocity radar frame, $\boldsymbol{D}(x,y)$ in which x and y are spatial coordinates and decomposes the signal into a series of orthonormal basis functions and spatial coefficients. The basis functions are referred to as modes. The shape of the mode is determined by the data itself and is not an assumed function *a priori*, as discussed in the previous section. The modes are ranked such that the first mode accounts for the most variance of the signal, the second mode – the second order contributor to the variance, and so-on. A summation of all the modes multiplied by the corresponding coefficients results in the reconstruction of the original measured signal exactly. A singular value decomposition is used to perform the POD:

$$\boldsymbol{D} = \boldsymbol{U\Sigma V^T} \tag{2}$$

where $\mathbf{U}$, $\boldsymbol{\Sigma}$, and $\boldsymbol{V}$ are matrices. The mode functions are encompassed in $\boldsymbol{V}$, and the diagonal elements of $\boldsymbol{\Sigma}$ are the singular values of matrix $\mathbf{D}$. Let $\boldsymbol{Q} = \boldsymbol{U\Sigma}$, then,

$$\boldsymbol{D} = \boldsymbol{QV^T} = \sum_{k=1}^{M} q_k v_k^T \tag{3}$$

where q_k are the spatial coefficients of the signal, and ${v_k}^T$ are the basis functions of the signal, or the proper orthogonal modes, and superscript T denotes transpose. The singular values occur in ranked order along the diagonal elements of $\boldsymbol{\Sigma}$ and signify the relative importance of each mode.

A low-order representation of the signal can be obtained by reconstructing the signal with a subset of the mode functions and spatial series coefficients. By associating particular modes with particular physical characteristics of the waves, this technique could be used to filter, or extract, the wave field signal from the radar measurements, which also contains contributions from other sources aside from the wave field. Some of these artifacts include: shadowing, sea-spikes, and range decay (e.g., Smith et al., 1996; Nieto Borge et al., 2004). Evaluation of whether or not the mode functions can be used as a filter in this way is a primary component of this research.

The reconstructed Doppler velocities, based on this sub selection of modes, is considered as one phase-resolved wave orbital velocity map. This procedure is applied to all radar frames in the time series (N); thus, the result is a time series of phase-resolved wave orbital velocity maps covering frames 1 to N. For purposes of comparison to the FFT-based approach only the results from frame 16 to N-16 are considered because the FFT-based approach requires use of a stack of 32 radar frames to generate one wave orbital velocity map.

Evaluation of POD Method

In this subsection POD wave orbital velocity reconstructions are compared to traditional dispersion curve filtering FFT-based methods (similar to that described in Young et al., 1985). Wave statistics from both methods are compared to "ground truth" buoy calculated statistics. Dependencies of wave statistics' accuracy on environmental conditions are examined, and phase-resolved velocity reconstructions are also compared to buoy measured velocity time series.

The reconstructed ocean wave-fields are characterized by three statistics: significant wave height (H_s), peak wavelength (λ_p), and root mean squared orbital velocity (V_{rms}). Conversion between orbital velocity and significant wave height is performed using linear wave theory for both the FFT-based and POD-based methods following the procedure described in Hackett et al. (2015). These three statistics are computed from 1D spectra and time series along the radar-identified peak wave direction. These statistics are computed along the peak wave direction because Doppler radar measures a projection of the total velocity along the radar look direction; thus, the measured Doppler velocity only contains all of the orbital velocity along the wave propagation direction. When two wave systems are present, two different bearings will contain the maximum orbital velocity for the wind seas and swell assuming they are not propagating in the same direction. Thus, we chose to compute the statistics along the radar identified peak wave direction with the understanding that any secondary wave system will only be encompassed as a projection of their orbital velocity along that (primary system) direction. This procedure is also adopted because in the conversion between orbital velocity and wave height it is assumed that the radar is looking into the wave propagation direction. These statistics are calculated for the "best" wave-field reconstruction using both reconstruction methods (i.e., FFT-based and POD-based). The best reconstruction for each method is defined as that which results in an H_s that most closely matches the buoy significant wave height statistic. Dispersion curve filter widths of $1\Delta\omega$ to

$10\Delta\omega$ for the dispersion filtering method and all possible leading mode reconstructions for the POD method were examined, and the best for each method was selected for comparison.

Figure 7a shows the best mode reconstruction (1 through n) versus the buoy measured significant wave height for all rotating radar datasets examined, which span a range of environmental conditions (see Table 3). The UM radar is marked in black dots and the radar developed by *Applied Physical Sciences, Inc.* (APS) under the ESMF program are denoted by magenta crosses. The best mode shows a weak trend with increasing significant wave height. Note that the majority of datasets are optimally reconstructed with fewer than the leading 20 modes (approximately 14% of the total modes). The low number of modes required for an accurate reconstruction could reduce storage demands for large datasets because only this subset of information must be saved. As wave height increases, the complexity of the wave field increases, presumably slightly increasing the number of required modes to accurately reconstruct the wave field.

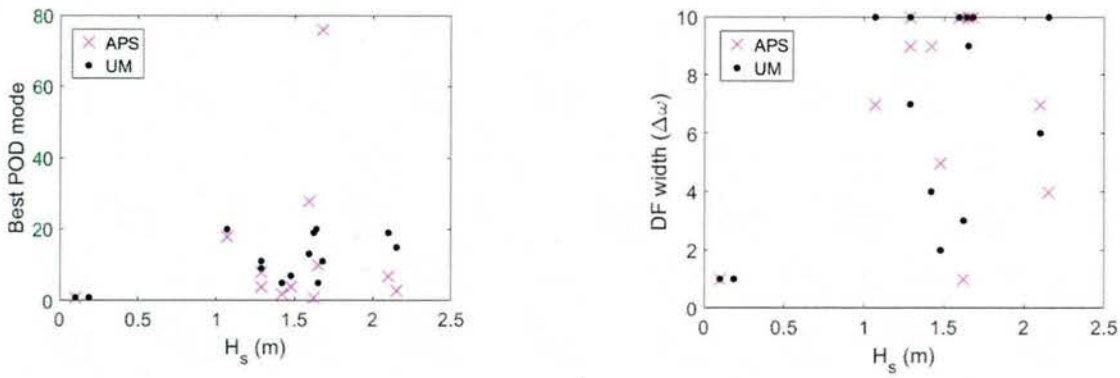

a b

Figure 7: (a) Most accurate mode (as evaluated by best match to buoy H_s) versus buoy measured H_s. (b) Most accurate dispersion filter width (as evaluated by best match to buoy H_s) versus buoy measured H_s.

Figure 7b shows the best dispersion curve filter width versus buoy measured significant wave height. Typically a filter width of $1\Delta\omega$ to $3\Delta\omega$ visually encompasses the majority of energy associated with the linear dispersion curve. However, this figure shows that in the majority of the datasets examined the most accurate reconstruction resulted from dispersion curve filtering widths greater than $3\Delta\omega$, and often at or near the upper limit of filter widths examined (i.e., $10\Delta\omega$). This result implies that some of the energy off of the linear dispersion curve is needed to obtain accurate H_s statistics when the H_s statistic is computed from 1D spectra along the peak wave propagation direction. Use of such a large dispersion curve filter width is unlikely to be chosen *a priori*.

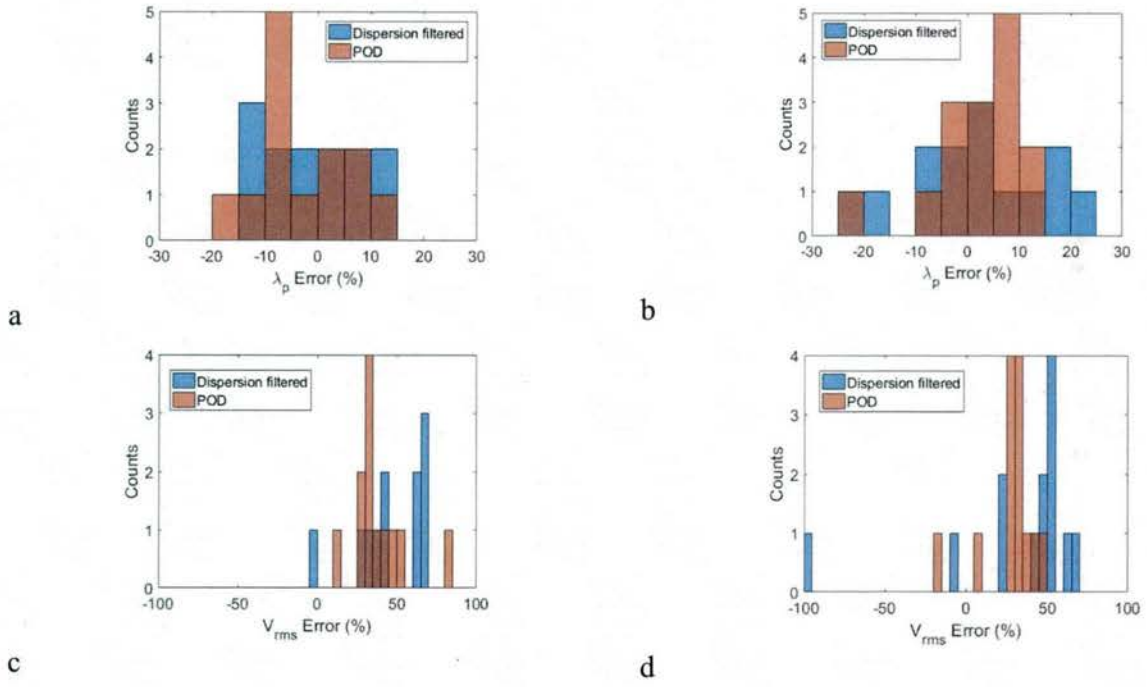

Figure 8: Histograms of the distribution of λ_p errors of POD-based orbital velocity reconstructions (orange) versus FFT dispersion filtered-based orbital velocity reconstructions (blue) for (a) the APS radar system and (b) the UM radar system. Lower panels show histograms of the distribution of V_{rms} errors for (c) the APS radar system and (d) the UM radar system.

Figure 8 shows histograms of the error of the peak wavelength (λ_p) and V_{rms} of the wave field reconstructions. The blue bars are FFT-based accuracies and the orange bars are for the POD-based results. Peak wavelengths are compared based-on the buoy identified dominant wave system when two wave systems were present. In such two wave system cases (see Table 3), particularly when the two systems were of similar magnitude, the buoy often measured the higher energy on the wind wave peak while the radar the swell peak. This discrepancy is likely due to the fact that the radar revisit rate to the same ocean patch results in a maximum observable frequency (Nyquist frequency) near the wind wave frequency peak, particularly when the ship had a non-negligible forward speed into the wave propagation direction. Thus, the radar is more sensitive to the swell, while the buoy is small in size (~0.5 m diameter) and is therefore sensitive to the wind seas. Panels (a) and (c) in Figure 8 shows the APS radar datasets and panels (b) and (d) show the UM datasets. This figure demonstrates that the majority of all reconstructions for both methods and radar systems are within less than 10% error in λ_p, and all datasets are within 25% error. This result confirms that both reconstruction methods are accurately capturing the buoy identified dominant wave system. The UM radar POD results appear more normally distributed and with a smaller spread compared to the APS radar POD results. The POD results also show greater frequency of lower λ_p errors than the dispersion filtered FFT-based results for both radars. The V_{rms} errors are greater in magnitude than the λ_p errors for both radars and both methods. These errors are larger because the V_{rms} is computed from time series along the peak wave direction as identified by the radar, which was often the swell for the reasons previously

discussed; while the buoy orbital velocity time series contains both swell and wind sea contributions (that are along different directions-see Table 3). Consequently, the wind sea contribution of the radar computed V_{rms} is often only a projection of the total wind wave orbital velocity along the peak swell direction. In other words, the buoy V_{rms} encapsulates both swell and wind seas while the radar V_{rms} is predominantly associated with the swell orbital velocities and only a projection of the wind sea component along the swell direction is included (when multiple wave systems existed). This explanation is further supported by the fact that the datasets with the lowest V_{rms} errors in Figure 8 are associated with one wave system datasets in Table 3. Nonetheless, the POD results in Figure 8 (c) and (d) show greater frequency of lower errors for both radars. Overall and generally, both methods performed similarly for both radars and both statistics with only slight differences in distribution and frequency of lower errors.

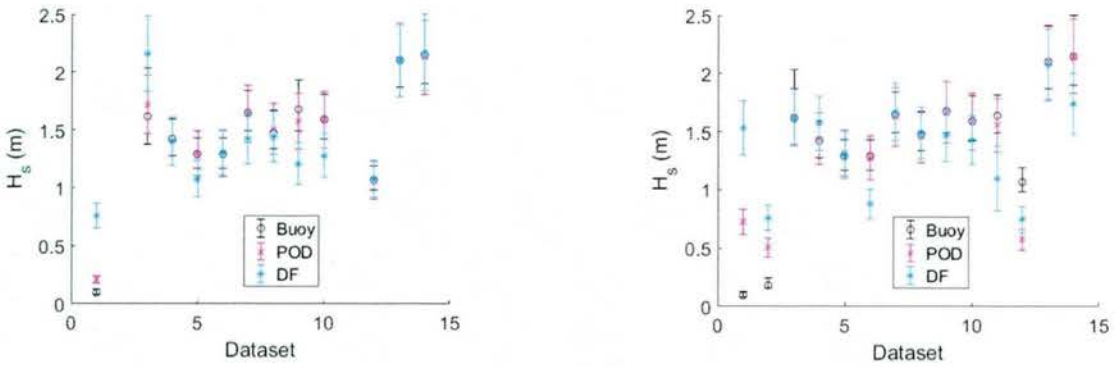

Figure 9: H_s POD-, dispersion filtered- (DF), and buoy-based estimates, with error bars, for (a) APS radar datasets and (b) UM radar datasets (see Tables 1 and 3).

Figure 9 shows the buoy, POD, and dispersion filtered estimated significant wave height with error bars calculated as described in the National Data Buoy Center (NDBC) manual (Earle, 1996). Panel (a) shows APS datasets and panel (b) shows UM datasets. For all datasets but the lowest H_s for the APS radar and the lowest three H_s for the UM radar, the POD H_s estimate falls within the error of the buoy measurement. The dispersion filtering method fails to accurately measure the significant wave height for the same datasets as the POD method as well as underestimates the significant wave height for an additional dataset for the UM radar system. Overall the POD and dispersion filtering methods perform comparably in terms of accurately estimating significant wave height, but the POD method is able to accurately estimate H_s for one more dataset than the FFT-based method. The large errors associated with the low wave height cases likely occur because of insufficient signal-to-noise ratios of the radar measurement.

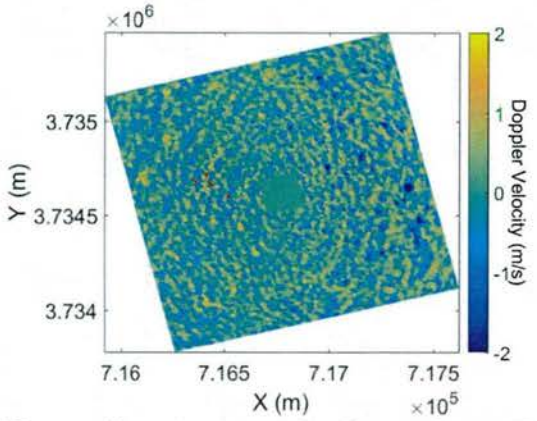

Figure 10: An example frame from UM radar dataset 8 with buoy tracks overlaid in red.

Relationships of wave statistics' accuracy (in terms of H_s, V_{rms}, and λ_p percent error) were examined with respect to various environmental conditions. The environmental conditions examined were wind speed (U_w), H_s, and λ_p (for swell and wind waves), V_{rms}, and the directional separation between swell and wind wave systems. However, no dependency of reconstruction accuracy with any specific environmental condition was identified, suggesting the accuracy of the POD method is not strongly dependent on the environmental conditions.

In summary, POD and dispersion filtered orbital velocity reconstructions were statistically comparable. Both methods accurately captured the buoy identified dominant wavelength, while the POD method and the UM radar appear to have slightly better λ_p accuracy. While both methods' H_s estimate is within the error bars of the H_s buoy measurement for the majority of cases examined, the dispersion filtering method failed to fall within the buoy H_s error bars one more time than the POD method.

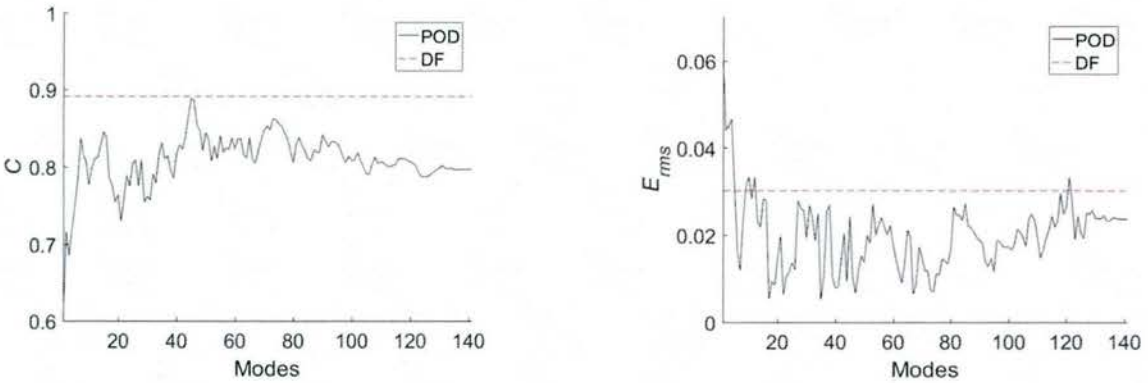

a b

Figure 11: (a) Correlation coefficient (C) between buoy time series and POD-based (black) orbital velocity time series versus number of modes used for the POD reconstruction. Also shown in red is correlation between the FFT-based DF orbital velocity time series and the buoy time series for the dispersion filter width that yielded the highest C (red). (b) Same as in (a) except showing root-mean-square error (E_{rms}) of orbital velocity in meters per second on the vertical axis. Results are for UM rotating radar dataset 7.

In order to characterize the phase accuracy of the wave-field reconstructions, comparisons to buoy time series are necessary. Radar reconstructed wave fields are geo-located and velocity time series of buoys as they travel through various range bins of the radar are compared. Figure 10 shows an example of a frame of UM Doppler velocity data and the overlaid buoy tracks within the radar field of view. Pearson's correlation coefficient (C) and root mean squared error (E_{rms}) are calculated between buoy velocity time series and the corresponding POD and dispersion filtered orbital velocity time series for each available instance when a buoy was within the field of view of the radar. The correlation and E_{rms}

statistics are calculated individually for each buoy-radar time series pair, and then averaged over all available buoys.

Figure 11 shows correlation and E_{rms} respectively for UM dataset 7 with three available buoy time series for comparison. The POD mode reconstruction with the highest correlation is essentially equal to that of the dispersion filter width with the highest C (shown as a red dashed line in Figure 11a), while the POD E_{rms} is lower for most mode reconstructions than E_{rms} for the dispersion filter width that produced the highest correlation. Overall, in this particular comparison, the two methods are fairly comparable in-terms of performance.

Figure 12 shows correlation and E_{rms} respectively for UM dataset 8 with four available buoy time series for comparison. For all POD mode reconstructions, the POD reconstruction correlation is significantly higher than the dispersion filter width with the highest correlation for this dataset. E_{rms} for the POD and dispersion filtering methods are within approximately 3 cm/s of each other, but the POD E_{rms} is slightly lower than that of the highest correlation dispersion filter width for all mode reconstructions.

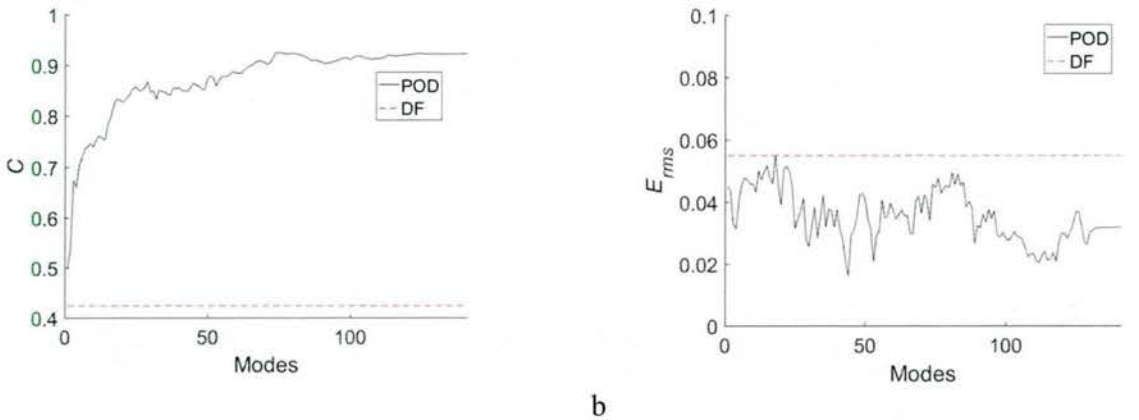

Figure 12: (a) Correlation coefficient between buoy orbital velocity time series and POD-based (black) orbital velocity time series versus number of modes used for the POD reconstruction. Also shown in red is correlation for the FFT-based DF orbital velocity time series for the dispersion filter width that yielded the highest correlation (red). (b) Same as in (a) except showing root-mean-square error of orbital velocity in meters per second on the vertical axis. Results are for UM rotating radar dataset 8.

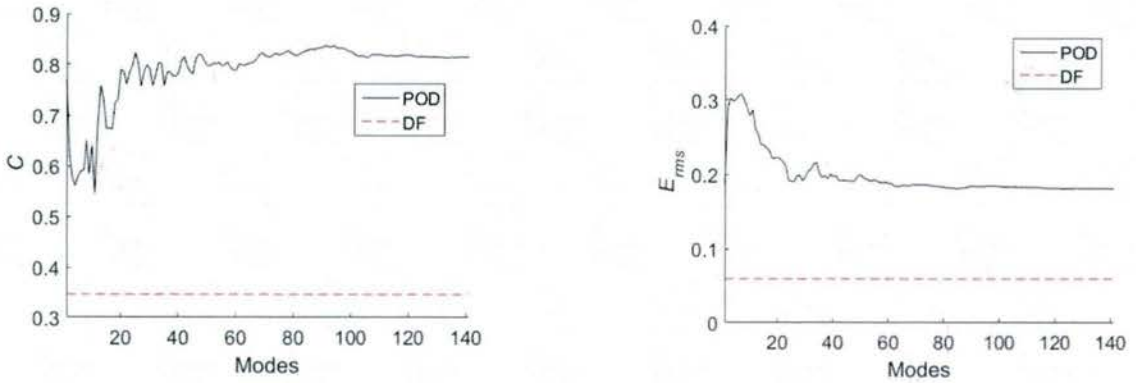

a b

Figure 13: (a) Correlation coefficient between buoy time series and POD-based (black) orbital velocity time series versus number of modes used for the POD reconstruction. Also shown in red is correlation coefficient for the FFT-based DF orbital velocity time series for the best dispersion filter width (red). (b) Same as in (a) except showing root-mean-square error of orbital velocity in meters per second on the vertical axis. Results are for APS rotating radar dataset 8.

Figure 13 shows the same results as in Figure 12 for APS radar dataset 8. Results show similar trends for the two radars except in the APS radar results the E_{rms} for the dispersion filtering results are lower than the POD results. For dataset 8, the POD performs much better than the dispersion filtering in terms of correlation for both radars, while RMS velocity errors are comparable for the UM radar, and POD-based results show errors that are more than twice as large as the dispersion filtering-based RMS velocity errors for the APS radar. Discrepancies between the correlation results and RMS velocity errors are attributed to errors resulting from phasing versus amplitude. In other words, correlation is high when the phasing of the waves is coherent between the two time series, while magnitudes of the orbital velocities are more accurate when E_{rms} is small. Thus, a high correlation and high E_{rms} implies that the phasing is accurate but the magnitude of the orbital velocities is either over or underestimated. Figure 14 (a)-(c) shows the k-ω spectrum for these three examples, where it is apparent that the group line in dataset 8 is significant relative to the energy on the dispersion curve (i.e., either greater or similar in magnitude), while the group line in dataset 7 is small in magnitude relative to the energy on the dispersion relationship.

Collectively, these results suggest that when group line energy is significant that dispersion curve filtering the data can result in inaccurate wave phasing, presumably because it does not adequately capture the interference effects associated with the group line energy (Plant and Farquharson, 2012). Conversely, the energy on the dispersion curve seems to impact most directly E_{rms} and the POD method does not isolate the energy on the dispersion curve causing the dispersion filtering method to outperform the POD method in a statistical sense (i.e., E_{rms}) over short time periods (~30 s). However, the statistical results previously shown indicate that over a larger period of time and space this effect is diminished because when examining statistics over several minutes (rather than ~30 s) the statistics from both methods were comparable. Figure 14 (d)-(f) shows an example k-ω spectral distribution for the best mode orbital velocity reconstruction (see Figure 7), where energy on and off the dispersion curve are clearly retained, but not all the energy on the dispersion curve is present in the reconstruction.

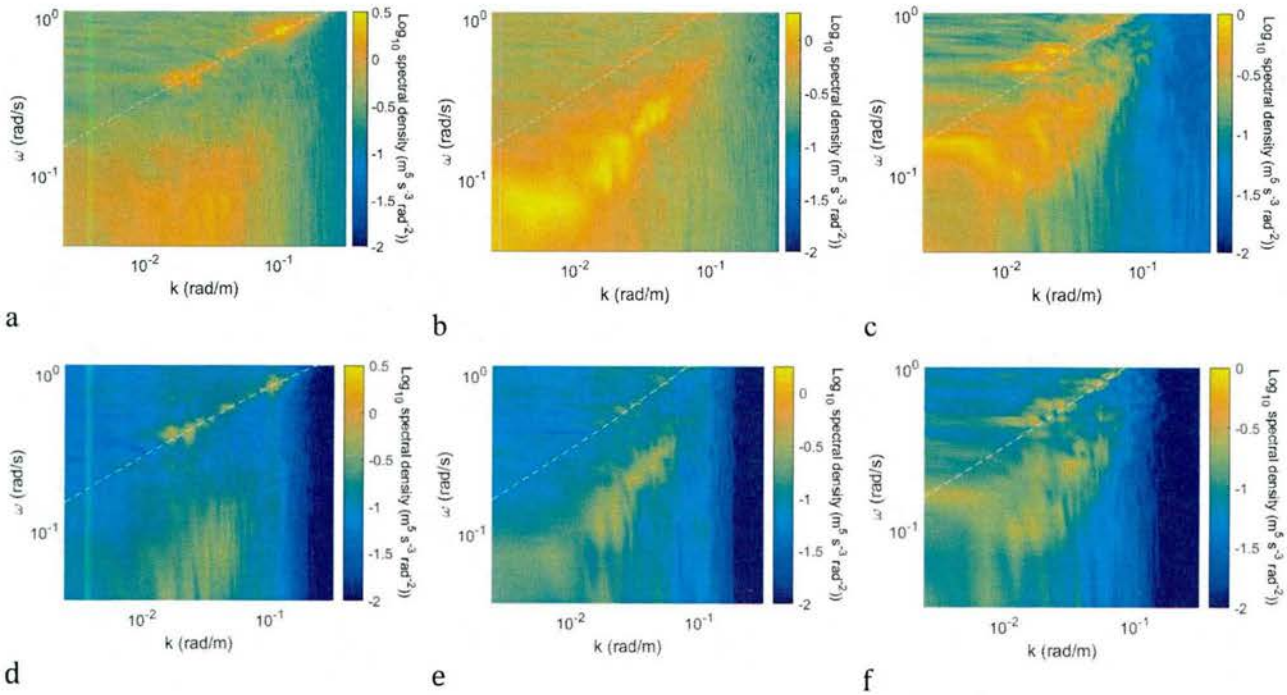

Figure 14: k-ω spectrum of Doppler velocity for (a) UM radar dataset 7, (b) UM radar dataset 8, and (c) APS radar dataset 8. k-ω spectrum for best mode orbital velocity reconstruction (see Figure 7) for (a) UM radar dataset 7, (b) UM radar dataset 8, and (c) APS radar dataset 8.

These sample phase-resolved results suggest that although the POD- and FFT-based results are statistically similar that there may be advantages to the POD method when determining phase-resolved ocean wave field maps. Improved performance of the POD-based method over the FFT-based method occurred most commonly when there was significant energy lying off the dispersion relationship for linear surface gravity waves (i.e., large group line energy).

The results from the radar emulator also support these conclusions. Figure 15 shows k-ω emulated Doppler velocity spectral distributions for an emulator run with and without a group line but that are otherwise identical. The group line appears due to increasing the magnitude of the orbital velocities to values large enough to generate wave field interference and breaking (those magnitudes are similar to the V_{rms} for dataset 13 in Table 3). By slightly lowering the orbital velocities (reduction by about $\sqrt{2}$), the interference effects are diminished and the group line is no longer apparent. Figure 15 (c) shows the average correlation coefficient, where the correlation coefficient is computed between POD reconstructed velocity time series and simulated wave orbital velocity (projected onto each direction) time series for each range bin and averaged over all range bins. This average correlation coefficient is computed for both emulator runs for all possible n mode reconstructions. Also shown is the average correlation coefficient for the dispersion filter width that produced the highest average correlation coefficient. Note that for the emulator run without a group line the optimal dispersion filter width is $1\Delta\omega$, while for the emulator run with a group line it is $10\Delta\omega$. This result is also consistent with the measured Doppler results, where larger dispersion filter widths are needed when group line energy is significant. Figure 15 (c) shows that when the group line energy is present that the POD-based average

correlation coefficient is higher than the optimal dispersion filtered correlation coefficient and the results are reversed for the emulator run without the group line. These results further support the conclusion that the POD-based method has advantages over FFT-based approaches in correctly estimating wave phase when group line energy is significant.

a b

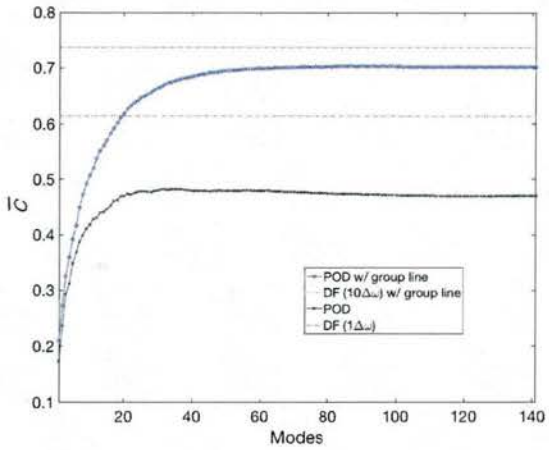

c

Figure 15: *k-ω* spectrum of Doppler velocity for (a) emulated UM radar measurements without a group line (b) emulated UM radar measurements with a group line, and (c) average correlation coefficient between POD-based reconstructed orbital velocities and simulated wave field orbital velocities for each *n* mode reconstruction along with the average correlation coefficient between dispersion filtered orbital velocities and simulated wave field orbital velocities for the dispersion filter width that produced the largest average correlation coefficient. See legend.

RESULTS

The primary knowledge gained in this research effort involves understanding the capabilities (advantages and disadvantages) non-Fourier based signal processing methods have for wave field retrieval from Doppler radar measurements. From a wave statistics viewpoint, the POD- and FFT-based wave retrieval methods performed similarly over a range of environmental conditions and for different radar systems. Because of the similar performance, POD-based methods could present advantages because they are more computationally efficient and can reduce data storage requirements. Data storage requirements are reduced because instead of storing all the information from the radar returns only a subset of information needs to be retained in order to recreate the relevant wave field information.

In terms of phase-resolved performance, the POD-based method presents advantages in more complex wave fields, specifically those that exhibit large energy levels off the dispersion relationship. The results of this study present evidence that at least part of this group line energy off the dispersion relationship is required in order to improve phase-resolved comparisons between Doppler radar-based orbital velocity maps and buoy orbital velocity time series. They also suggest that at least part of the energy within the group line is important and related to the wave field as demonstrated in the numerical study of Plant and Farquharson (2012). Because the entire wave field retrieval in a POD-based method occurs in the spatiotemporal domain, use of this method can be more efficient because one does not need to consider time series duration as is required for FFT-based methods due to its dependence on spectral resolution. The primary disadvantage of the POD method is that a clear cut-off for the mode selection was not obvious *a priori*; however, a rigorous evaluation of how to perform this mode selection was not performed in this study. Thus, future work extending this capability should focus on development of methods to optimize the mode selection. However, it should be noted that in most of the data sets examined in this study the mode subset needed to most accurately reconstruct the wave field statistically required less than 15% of all the modes.

IMPACT/APPLICATIONS

In many applications, such as intra- and inter-ship transfers, helicopter landing, crane operations, and small boat launch and recovery operations, information about the wave field surrounding a ship would enhance safety and increase the operational envelope of such activities. In addition, such information would generally increase maritime domain awareness. For example, shore-based or drone-based radars in key areas could provide quantitative insight into ocean surface conditions that cannot be directly observed. Improvement of signal processing methods applied to sea clutter helps facilitate the development and robustness of such capabilities. Finally, there are many scientific research areas that would also be benefited by knowledge of the spatial distribution of ocean surface waves over large areas such as research on: rogue waves, ocean wave development and growth, and wave-wave energy exchange and interactions.

RELATED PROJECTS

ONR's ESMF FNC is directly related to this research (e.g., Connell et al., 2015; Alford et al., 2015). The PI collaborated with other researchers in this community for this research. This involvement included use of data collected in several tests and experiments conducted for this program, use of simulations developed for this program, and participation at ESMF workshops and review meetings. PI Hackett presented results of this study to the ESMF FNC community during review meetings to keep them apprised of results.

REFERENCES

Alford, A. K., Lyzenga, D., Beck, R. F., Nwogu, O., Johnson, J. T., and A. Zundel, 2015, A real-time system for forecasting extreme waves and vessel motions, *Prof. Robert F. Beck Honoring Symposium on Marine Hydrodynamics*, 11, American Society of Mechanical Engineers (ASME). doi: 10.1115/OMAE201542420.

Chatterjee, A, 2000, An introduction to the proper orthogonal decomposition, *Current Science*, 78, 808-817.

Connell B.H., Rudzinsky J.P., Brundick C.S., Milewski W.M., Kusters J.G., and G. Farquharson, 2015, Development of an environmental and ship motion forecasting system. ASME. International Conference on Offshore Mechanics and Arctic Engineering, *Prof. Robert F. Beck Honoring Symposium on Marine Hydrodynamics*, 11, American Society of Mechanical Engineers (ASME). doi:10.1115/OMAE2015-42422.

Diamessis, P.J., Gurka, R., and A. Liberzon, 2010, Spatial characterization of vortical structures and internal waves in a stratified turbulent wake using proper orthogonal decomposition, *Physics of Fluids*, 22, doi:10.1063/1.3478837.

Earle, M.D., 1996, Nondirectional and directional wave data analysis procedures, *NDBC Technical Document 96-01*, Stennis Space Center, US Department of Commerce, National Oceanic and Atmospheric Administration, and National Data Buoy Center.

Hackett, E.E., C.F. Merrill, and J. Geiser, 2014, The application of proper orthogonal decomposition to complex wave fields, *Proceedings of the 30th Symposium on Naval Hydrodynamics*, Hobart, Australia.

Hackett, E.E., A.M. Fullerton, C.F. Merrill, and T.C. Fu, 2015, Comparison of incoherent and coherent wave field measurements using dual-polarized pulse-Doppler X-band radar, *IEEE Trans. Geosci. Remote Sens.*, 53, 11, 5926-5942.

Kammerer, A.J., 2017, The application of proper orthogonal decomposition to numerically modeled and measured ocean surface wave fields remotely sensed by radar, *M.S. Thesis*, Coastal Carolina University.

Kerschen, G., and J. C. Golinval, 2002, Physical interpretation of the proper orthogonal modes using the singular value decomposition, *Journal of Sound and Vibration*, 249, 5, 849-865.

Nieto Borge, J. C., Rodriguez, G. R. Hessner, K. and P. I. Gonzalez, 2004, Inversion of marine radar images for surface wave analysis, *Journal of Atmospheric and Oceanic Technology*, 21, 1291-1300.

Plant, W. J., and G. Farquharson, 2012, Origins of features in wavenumber-frequency spectra of space-time images of the ocean, *Journal of Geophysical Research*, 117, 1-10.

Smith, M. J., Poulter, E. M. and J. A. McGregor, 1996, Doppler radar measurements of wave groups and breaking waves, *Journal of Geophysical Research*, 101, 14269-14282.

Young, I. R., W. Rosenthal, and F. Ziemer, 1985, A three-dimensional analysis of marine radar images for the determination of ocean wave directionality and surface currents, *Journal of Geophysical Research*, 90, C1, 1049-1059.

PUBLICATIONS

Hackett, E.E., A.M. Fullerton, C.F. Merrill, and T.C. Fu, 2015, Comparison of incoherent and coherent wave field measurements using dual-polarized pulse-Doppler X-band radar, *IEEE Trans. Geosci. Remote Sens.*, 53, 11, 5926-5942. [referred, published]

Kammerer, A.J., 2017, The application of proper orthogonal decomposition to numerically modeled and measured ocean surface wave fields remotely sensed by radar, *M.S. Thesis*, Coastal Carolina University.

EDUCATION

One graduate student was educated under funding from this grant that is expected to graduate in May 2017.